Available online at www.sciencedirect.com
SCIENCE DIRECT®
Journal of Power Sources 139 (2005) 79–90
JOURNAL OF POWER SOURCES
www.elsevier.com/locate/jpowsour

In situ visualization study of CO_2 gas bubble behavior in DMFC anode flow fields

H. Yang, T.S. Zhao*, Q. Ye

Department of Mechanical Engineering, The Hong Kong University of Science & Technology, Clear Water Bay, Kowloon, Hong Kong SAR, China

Received 20 April 2004; accepted 19 May 2004
Available online 2 September 2004

Abstract

This paper reports on a visual study of the CO_2 bubble behavior in the anode flow field of an in-house fabricated transparent Direct Methanol Fuel Cell (DMFC), which consisted of a membrane electrode assembly (MEA) with an active area of $4.0 \times 4.0\,cm^2$, two bipolar plates with a single serpentine channel, and a transparent enclosure. The study reveals that at low current densities, small discrete bubbles appeared in the anode flow field. At moderate current densities, a number of gas slugs formed, in addition to small discrete bubbles. And at high current densities, the flow field was predominated by rather long gas slugs. The experiments also indicate that the cell orientation had a significant effect on the cell performance, especially at low methanol flow rates; for the present flow field design the best cell performance could be achieved when the cell was orientated vertically. It has been shown that higher methanol solution flow rates reduced the average length and the number of gas slugs in the flow field, but led to an increased methanol crossover. In particular, the effect of methanol solution flow rates on the cell performance became more pronounced at low temperatures. The effect of temperature on the bubble behavior and the cell performance was also examined. Furthermore, for the present flow field consisting of a single serpentine channel, the channel-blocking phenomenon caused by CO_2 gas slugs was never encountered under all the test conditions in this work.
© 2004 Elsevier B.V. All rights reserved.

Keywords: Fuel cell; DMFC; MEA; Methanol; Flow visualization; Two-phase flow

1. Introduction

It has recently been shown that the opportunity in terms of market size and growth rate for small fuel cells for portable electronic devices is commercially compelling as compared with batteries [1]. Since methanol has a higher energy density under ambient conditions and can be processed and stored more easily than a gas fuel, a liquid fed direct methanol fuel cell (DMFC) is becoming a potential power source potable applications [2,3]. For this reason, the DMFC is now being studied by a number of university researchers and industry engineers all over the world [4–20].

The DMFC consists of a proton exchange membrane with an anode and a cathode catalyst layer on each side. Gas diffusion layers, usually made of carbon paper or carbon cloth, are used to cover the catalyst layers and form the membrane electrode assembly (MEA). The MEA is then sandwiched between two current collectors that have some flow channels machined into the surface for the supply of fuel and oxidant. Typically, the DMFC is operated at a temperature lower than 100 °C. At the anode, methanol is electrochemically oxidized to CO_2, while at the cathode, oxygen is reduced to water: the electrochemical reactions taking place in the cell are described as follows:

$$CH_3OH + H_2O \rightarrow CO_2 + 6H^+ + 6e^- \text{ (anode reaction)} \quad (1)$$

$$\tfrac{3}{2}O_2 + 6H^+ + 6e^- \rightarrow 3H_2O \text{ (cathode reaction)} \quad (2)$$

which can be combined to give the overall reaction as:

$$CH_3OH + \tfrac{3}{2}O_2 \rightarrow 2H_2O + CO_2 \quad (3)$$

Thus, the overall cell reaction is the electro-oxidation of methanol to CO_2 and water. Apparently, all the reaction products, gas CO_2 at the anode and liquid water at the cathode, should be removed from the electrode structure and cell as efficiently as possible to maintain an effective continuous reaction. Like the water management at the cathode, the efficient removal of CO_2 at the anode is one of the most important research issues in the development of DMFCs.

In the DMFC, methanol solution is fed into the anode flow field and diffuses to the catalyst sites through the gas

* Corresponding author. Tel.: +852 2358 8647; fax: +852 2358 1543.
E-mail address: metzhao@ust.hk (T.S. Zhao).

0378-7753/$ – see front matter © 2004 Elsevier B.V. All rights reserved.
doi:10.1016/j.jpowsour.2004.05.033

diffusion layer, while the reaction-produced gas CO_2 at the catalyst layer transport backward into the anode channels through the gas diffusion layer. As such, a counter liquid–gas two-phase flow takes place in the diffusion layer. Since, the quantity of CO_2 increases with increasing the current density, at high current densities, the volume fraction of CO_2 in the anode flow field becomes rather large. Under such a situation, CO_2 removal from the catalyst sites is critical to ensure availability of an adequate surface area for methanol oxidation. To this end, CO_2 has to be removed effectively from both the diffusion layer and the anode flow field. Otherwise, CO_2 gas slugs accumulated in the anode flow field may not only hinder the methanol transport to the catalyst sites, but also cause a higher pressure in the anode flow field, leading to an increase in methanol crossover. Thus, research on two-phase flow characteristics of gas CO_2 and methanol solution in the anode flow field is essential for the design and optimization of a DMFC.

Relatively, few papers have been reported on the study of CO_2 bubble behavior in the anode flow field of DMFCs. Mench et al. [21] examined gas bubble growth and ejection from the backing layer/flow channel interface region with video microscopy and observed discrete bubbles of the order of 0.1–0.5 mm evolving from various locations within the backing layer. Argyropoulos et al. [22] studied the CO_2 flow characteristics in a DMFC with the aid of a high-speed video camera and found three flow patterns including bubbly, slug and annular flow in practical fuel cell operation conditions. In their experiments, they tested two different flow field designs: one consisted of parallel channels having a cross-section area of $2.0 \times 2.0\,mm^2$ and a length of 30.0 mm; the other consisted of cross flow channels having the same size, but including a triangular enlarging inlet and outlet sections. They studied the effects of the current density and the methanol solution flow rate and found that gas slugs at low flow rates and high current densities blocked the flow channels. Scott et al. [23] visually investigated the CO_2 gas evolution and flow behavior with flow beds based on stainless steel mesh. In their works, a number of the flow designs, based on stainless steel mesh, showed promising behavior in terms of gas removal characteristics and electrical performance. Bewer et al. [24] reported a novel method simulating two-phase flow in a DMFC using an aqueous H_2O_2 solution. The influence of the flow-field on the bubble formation and on the flow homogeneity, as well as the influence of manifold on the flow homogeneity was investigated.

In this paper, we present a visual investigation of CO_2 gas bubble behavior in a transparent DMFC with its anode flow field consisting of a single serpentine channel. The in situ taken images show that there exist various CO_2 gas bubble flow patterns at different current densities. Effects of various operation parameters, including methanol solution flow rate, cell orientation, and cell operating temperature, on the cell performance and the two-phase flow characteristics in the anode flow field were examined.

2. Experimental

2.1. Transparent cell

A transparent DMFC was designed and fabricated for this visualization study, as schematically shown in Fig. 1. The MEA detailed in the subsequent paragraph, was sandwiched between two bipolar plates with a gasket onto either side of the MEA. This assembly, including the bipolar plates and MEA, was clamped between two enclosure plates by eight M8 screw joints, each having a torque of about 3 Nm.

The MEA, fabricated in this work, had an active area of $4.0 \times 4.0\,cm^2$ and consisted of two single-side ELAT electrodes from E-TEK and a Nafion® membrane 115. Both anode and cathode electrodes used carbon cloth (E-TEK, Type A) as the backing support layer with 30% PTFE wet-proofing treatment. The catalyst loading on the anode side was $4.0\,mg\,cm^{-2}$ with unsupported [Pt:Ru] Ox (1:1 a/o), while the catalyst loading on the cathode side was $2.0\,mg\,cm^{-2}$ using 40% Pt on Vulcan XC-72. Furthermore, $0.8\,mg\,cm^{-2}$ Nafion® was applied onto the surface of each electrode. The Nafion® membrane 115, before being used, was first cleaned following a standard procedure: (i) boiling membrane in 5 wt.% H_2O_2 solution of 80 °C for 1 h; (ii) rinsing with DI water of 80 °C for 1 h, (iii) boiling membrane in 0.5 M H_2SO_4 solution of 80 °C for 1 h, and (iv) rinsing with DI water of 80 °C for 1 h. Finally, the MEA was formed by hot pressing at 135 °C and 5 MPa for 3 min.

To avoid corrosion, the bipolar plates, shown in Fig. 2, were made of 316 stainless steel [25–28] plates with a thickness of 2.0 mm. As can be seen in Fig. 2, the rectangular bipolar plate consisted of two portions, the channel area and the extension area. The channel area acted as the distributor for supplying fuel and oxidant to the MEA, in which a single serpentine channel, $2.0 \times 2.0\,mm^2$, was machined by the

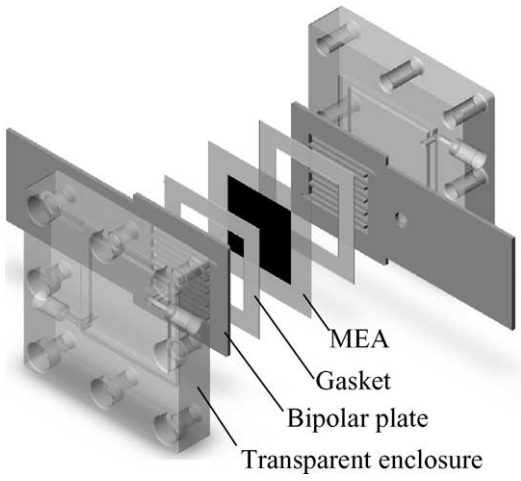

Fig. 1. Transparent DMFC.

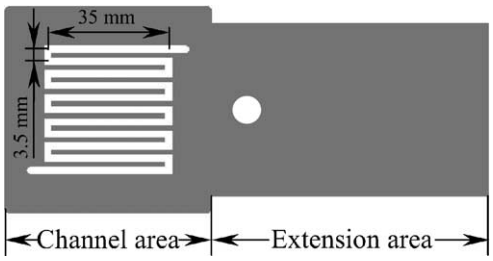

Fig. 2. Flow field and the current collector.

wire-cut technology. The width of the ribs was 1.5 mm. The serpentine channel, having a total length of 420 mm, consisted of 11 serially-linked horizontal segments (35.0 mm long) and 10 vertical segments (3.5 mm long). The extension area of the bipolar plates served as a current collector. In addition, a tape heater was attached to the extension area to adjust the cell operating temperature to a desired value during the experiments.

For the purpose of visualization, the two enclosure plates, each having a thickness of 4.0 cm, were made of transparent Lucite material. Through the transparent enclosure plate, two-phase flow characteristics of gas CO_2 and methanol solution in the anode flow field could be distinctly visualized and recorded by the image recording system. It is worth pointing out that the transparent Lucite material, having a well-insulated property, can effectively keep the heat in the MEA and the bipolar plates from dissipating to the surroundings under the condition of higher operation temperatures.

2.2. Test loop

The experiments were carried out in the test loop shown in Fig. 3. Methanol solution was driven by a digital HPLC micro-pump (Series III), which can precisely control the liquid flow rate from 0.01 to 10.0 ml min^{-1} with an error of 2% of reading. Before entering the cell, methanol solution was pre-heated to a desired temperature by a heater connected to a temperature controller. The mixture of gas CO_2 and unreacted methanol solution was drained from the cell and cooled down when passing through a cooling system. Gas CO_2 was separated from the mixture and released to atmosphere, while the unreacted methanol solution was re-collected into a chemical liquid tank. Simultaneously, high purity oxygen of 99.999% as oxidant was provided to the cathode side of the cell without humidification. The flow rate of oxygen was controlled and measured by a mass flow meter (Omega FMA-7105E) combined with a multiple channel indicator (Omega FMA-5876A), which can control the oxygen flow rate from 0 to 500 standard cubic centimeter per minute (SCCM) with an error of 1% of full scale. Similar to methanol solution, oxygen gas was also pre-heated to the desired temperature, and then flowed into the cathode side of the cell. Liquid or gaseous water would be produced depending on the oxygen flow rate and cell working temperature. With the help of another cooling system, water was condensed and collected to the chemical liquid tank, and the excess oxygen gas was released to atmosphere.

In addition, a purge system and a degas system were built in the present test loop. Prior to each new test, the gas purge system was used to sweep out the residual fuel and oxidant

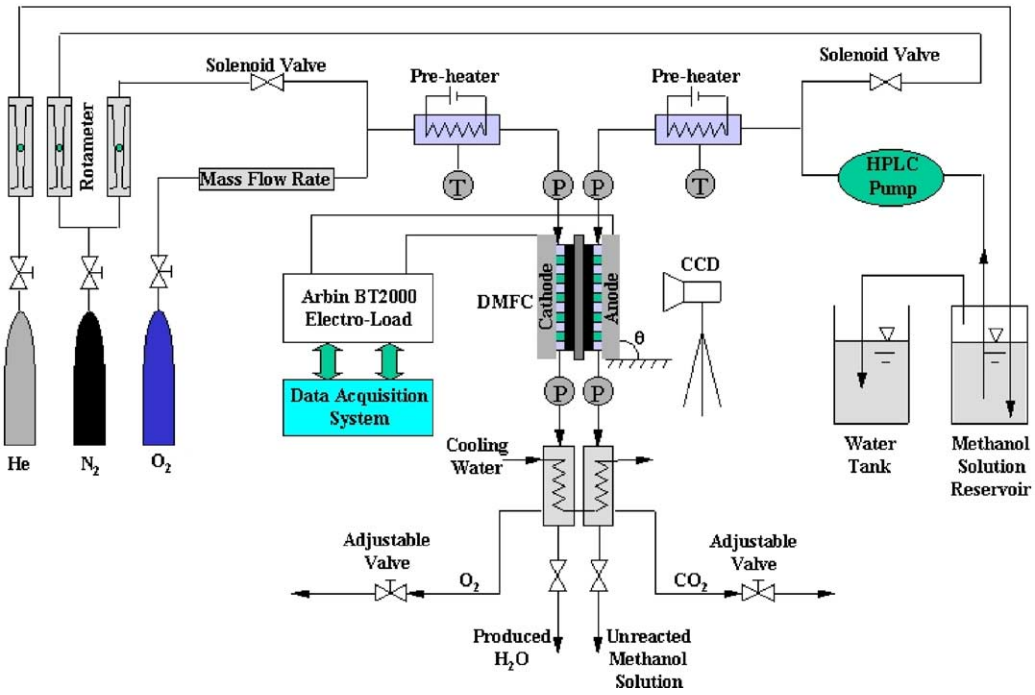

Fig. 3. Schematic of the DMFC test loop.

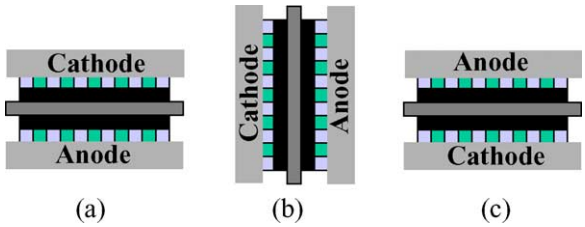

Fig. 4. Cell orientations: (a) horizontal orientation with the anode below the MEA ($\theta = 0°$); (b) vertical orientation ($\theta = 90°$); (c) horizontal orientation with the anode above the MEA ($\theta = 180°$).

in the cell using nitrogen gas. In order to prevent methanol solution from exposing to atmosphere, resulting in fuel deterioration, the degas system was used to inject helium gas into the closed methanol solution tank during the experiments.

2.3. Image recording system

A video and photo imaging system, including a JVC CCD, a NAVITAR 6X CCD C-Mount Len and a digital camcorder (SONY DCR-TRV900E), was employed to capture the images of the two-phase flow characteristics of gas CO_2 and methanol solution in the anode flow field. Being zoomed in by the NAVITAR 6X CCD C-Mount Lens, the images of the anode flow field were shot by the JVC CCD and recoded on a mini digital video cassette by the digital camcorder. A shutter speed of 1/10,000 s and a recording speed of 25 frames/s were selected to visualize and record each flow pattern. A 600-W spotlight (ARRILITE 600) was employed to meet the lighting requirement for capturing images at the high shutter speed of 1/10,000 s. The bubble velocity was measured from consecutive images of the bubble replayed in slow motion, and was calculated based on the time interval of 1/25 s for the bubble to travel a given distance.

2.4. Electrochemical instrumentation and test conditions

In this work, an Arbin BT2000 electro-load interfaced to a computer was employed to control the cell operation condition and to measure voltage-current (polarization) curve. A pre-written schedule program was run to realize the control and measurement for a desired test condition. In this schedule program, the control mode such as current or voltage discharge, the accurate discharging value and duration, and data-sampling period were set in detail. All the tests in this work were conducted by selecting current discharge as control mode and scanning the current value from zero (i.e., open circuit) to a possible maximum value with an increment of 0.16 A (i.e., 10 mA cm^{-2} for the present MEA area of 4.0 × 4.0 cm^2) each step.

All the experiments reported in this work were performed at the same cathode operation condition, i.e. a constant oxygen gas flow rate of 100 SCCM and atmospheric pressure (0.1 MPa). As shown in Fig. 4, the experiments were performed for three different cell orientations: vertical orientation ($\theta = 90°$), horizontal orientation with the anode below the MEA ($\theta = 0°$), and horizontal orientation with the anode above the MEA ($\theta = 180°$).

3. Results and discussion

3.1. General observation of the CO_2 gas bubble behavior

The images of the CO_2 gas bubble behavior in the anode flow field corresponding to various operation conditions are shown in Figs. 6, 8, 12 and 16. Thanking to the reflection of liquid–gas interface, the CO_2 bubble formation, growth, and departure from the surface of the gas diffusion layer and their motions in the flow channel were distinctly captured by the image recording system. As can be seen from these images, with the help of lighter liquid–gas interface, gas bubbles can be easily distinguished from liquid methanol solution. The region enveloped by a lighter-grey liquid–gas interface represents a gas area, whereas the rest region in the flow field is the liquid area.

In this work, we observed that the formation of CO_2 gas bubbles was not uniform over the surface of the gas diffusion layer: at some sites, gas bubbles were generated continuously, whereas at the other sites, no bubble occurred at all. This non-uniform distribution of bubbles is attributed to the fact that both the diffusion layer and the catalyst layer cannot be fabricated with perfect uniform surfaces. At each active nucleation site, we found that gas bubble formed, grew, and departed from the surface of the diffusion layer with the help of the crosscurrent flowing methanol solution. As such, for a given operation condition, a process of bubble formation and departure repeated periodically. After departing from the surface of the gas diffusion layer, gas bubbles, usually small and in a spherical shape, traveled upwards to the upper surface of the channel due to buoyancy, and moved towards the outlet of the flow field with liquid methanol solution. Traveling along the flow channel towards the outlet, the bubbles gradually grew up due to coalescing with the newly produced small bubbles from the surface of the gas diffusion layer.

Fig. 5 presents the cell polarization behavior and the power output for the case when the cell was oriented vertically ($\theta = 90°$) and with 1 M methanol solution supplied at a flow rate of 1.0 ml min^{-1} at 60 °C. The images of the CO_2 bubble behavior for selected current densities, corresponding to Point A to F in Fig. 5, are shown in Fig. 6. A progressive scan of the six images shown in Fig. 6 indicates that the quantity of gas CO_2 bubbles in the flow field increased progressively as the current density was increased from 10 to 200 mA cm^{-2}. The increase in the quantity of CO_2 bubbles with increasing the current density can be readily explained from the following equation:

$$q_{CO_2} = \frac{AM_{CO_2}}{6F\rho_{CO_2}} i \tag{4}$$

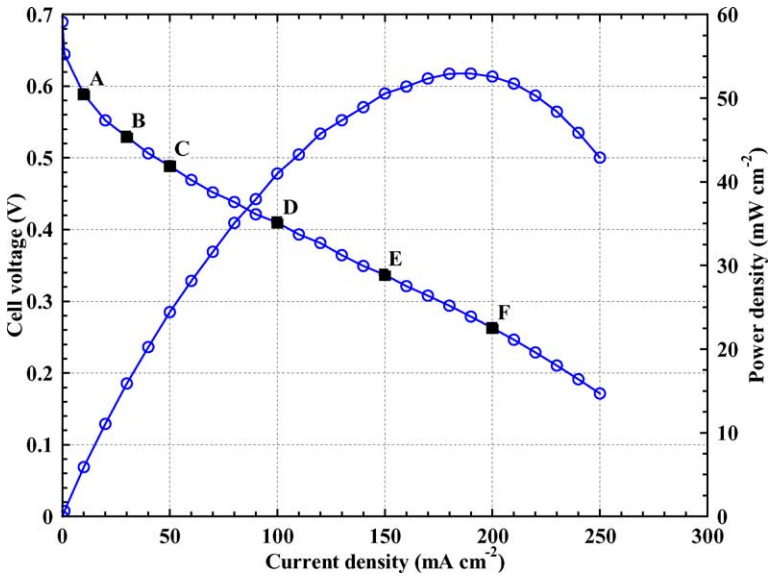

Fig. 5. Cell performance for the vertical orientation ($\theta = 90°$) with 1 M methanol solution fed at 1.0 ml min^{-1} and at 60 °C.

where q_{CO_2} represents the volume of gas CO_2 and A is the MEA area. At low current densities (e.g. 10 mA cm^{-2}), as can be observed from the image for Point A, a rather small number of discrete gas bubbles were generated and present in the flow field. Therefore, at low current densities, the two-phase flow pattern can be regarded as bubbly flow [29] over the entire flow field. It is also worth mentioning that when the current density was sufficiently low (less than 5 mA cm^{-2} for the cell in this work), no CO_2 gas bubble was observed over the entire flow field. This phenomenon is attributed to the fact that rather small quantity of gas CO_2 was produced, which might completely be dissolved in the aqueous methanol solution [30]. With the increase in the current density, as seen from the images for Point B and C, some of small spherical bubbles grew up with a fast growth rate and eventually became slug bubbles, which have a semi-spherically shaped head and tail, flat at top and bottom boundaries. Unlike the small spherical bubbles, slug bubbles usually were long and spanned the entire channel cross-section. As a result, bubbly flow transitioned to slug flow [29] in the middle region of the flow field, and bubbly flow and slug flow coexisted in the flow field. With

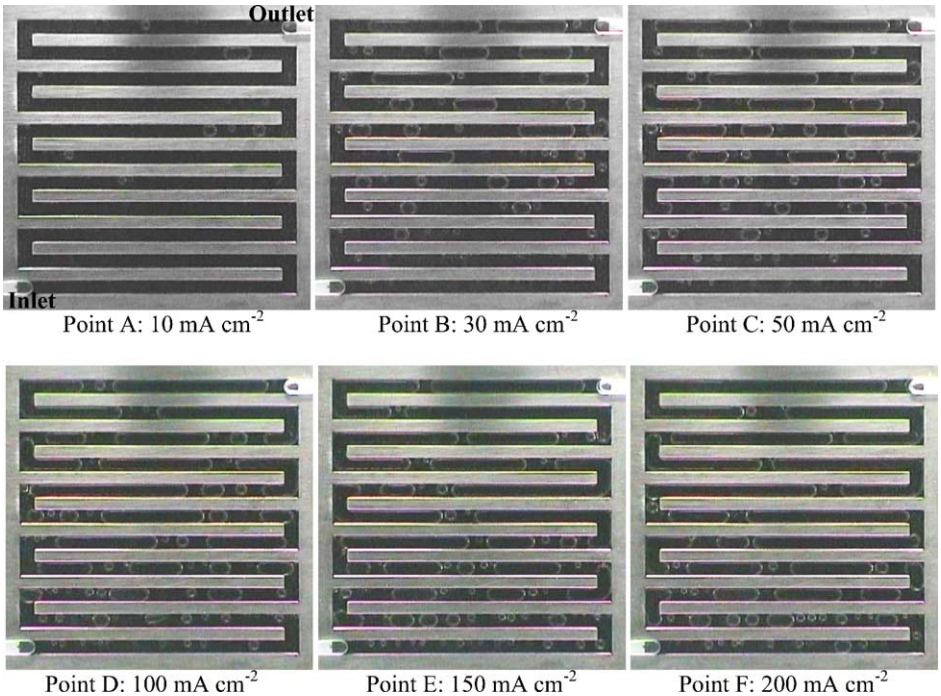

Fig. 6. CO_2 bubble behavior at different current densities for the vertical orientation ($\theta = 90°$) with 1 M methanol solution fed at 1.0 ml min^{-1} and at 60 °C.

the further increase in the current density, as seen from the images for Point D to F, slug flow was present almost in entire flow field, and bubbly flow was only observed in the entrance region of the flow field. It is important to note from the image for Point F that at high current densities, rather long gas slugs formed and occupied almost the entire channel cross section, causing the effective contact area between the liquid fuel and the gas diffusion layer to be extremely small. Under such a situation, the long gas slugs may restrict the continuous supply of methanol through the gas diffusion layer to the catalyst surface, eventually leading to deterioration of methanol mass transfer. During the experiments, we also found that for the cases when the current density exceeded 200 mA cm^{-2}, the CO_2 bubble behavior in the flow field exhibited no significant difference as compared with the case for $i = 200$ mA cm^{-2}. For liquid–gas two-phase flows, the variation in flow patterns is rather sensitive to the change in the gas void fraction at intermediate values. However, as the gas void fraction is sufficiently high or low (high or low current densities), the change in the flow patterns becomes less sensitive to the gas void fraction. In addition, at high current densities, a further increase in the quantity of gas CO_2 only leads to a negligible change in void fraction due to the increase in the gas-liquid slip ratio [31].

It is worth mentioning that for the present flow field consisting of a single serpentine channel, the channel-blocking phenomenon caused by CO_2 gas slugs was never found under all the test conditions in this work, although this phenomenon was found in the flow field consisting of parallel channels in the work by Argyropoulos et al. [22]. For the present flow field design with a single serpentine channel, there is no flow dead end; for a given flow rate, gas slugs may cause an increase in the pressure drop but can never block the channel.

3.2. Effect of cell orientations

The effect of cell orientations on the cell performance for the case when 1 M methanol solution was fed at 0.5 ml min^{-1} and at 60 °C is shown in Fig. 7. It is clear from this figure that the cell orientation has a significant effect on the cell performance, especially in the mass transport limitation region: the best performance was achieved when the cell was orientated vertically ($\theta = 90°$); the performance became worse when the cell was orientated horizontally with either the anode below the MEA ($\theta = 0°$) or the anode above the MEA ($\theta = 180°$). Let us now turn our attention to the CO_2 gas bubble behavior for different cell orientations at a selected current density (150 mA cm^{-2}), as shown in Fig. 8. It is found from Fig. 8 that more long gas slugs formed in the flow field for the cases of $\theta = 0°$ and $\theta = 180°$, whereas for the case of $\theta = 90°$, the number of the long gas slugs was reduced. The effect of the cell orientation on the CO_2 gas bubble behavior is attributed to buoyancy force. For the vertical orientation, buoyancy force assists the removal of CO_2 gas bubbles on the top of the forced circulation of methanol solution, thereby tending to suppress the formulation of long gas slugs. However, as the cell was oriented horizontally, the effect of buoyancy became small, tending to accumulate gas bubbles in the flow field and eventually to form long gas slugs. We estimated the bubble velocity by analyzing the recorded video and found that gas bubbles moved faster for the case of $\theta = 90°$ than for the cases of $\theta = 0°$ and $\theta = 180°$. For instance, at the current density of 150 mA cm^{-2}, the bubble velocity in the exit region was about 55.7 mm s^{-1} for the case of $\theta = 90°$, whereas it was reduced to 48.7 and 50.0 mm s^{-1} for the cases of $\theta = 0°$ and $\theta = 180°$, respectively. Therefore, it can be concluded that the higher cell performance for the case of the vertical

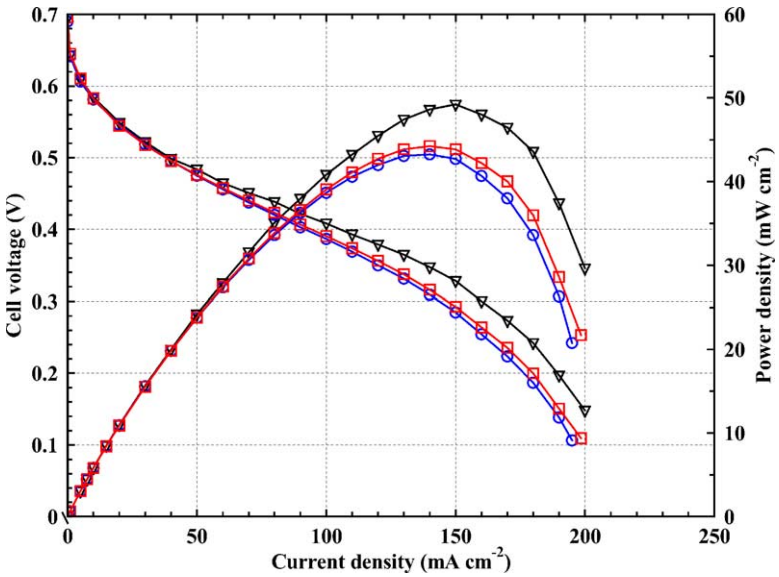

Fig. 7. Effect of cell orientation on the cell performance with 1 M methanol solution fed at 0.5 ml min^{-1} and at 60 °C (○, $\theta = 0°$; □, $\theta = 180°$; ▽, $\theta = 90°$).

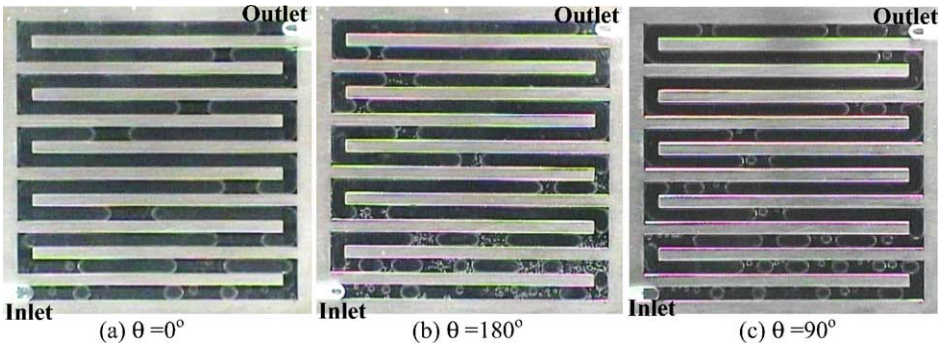

Fig. 8. CO_2 bubble behavior for different cell orientations at current density of 150 mA cm^{-2} and with 1 M methanol solution fed at 0.5 ml min^{-1} and at 60 °C.

orientation shown in Fig. 7 is due to buoyancy force, which assists the removal of gas bubbles in the flow field.

It is also interesting to note from Fig. 7 that the horizontal cell orientation with the anode above the MEA ($\theta = 180°$) gave better performance than with the anode below the MEA ($\theta = 0°$). This phenomenon can be explained as follows. For the horizontal cell orientation with the anode above the MEA ($\theta = 180°$), bubbles generated from the lower catalyst layer, penetrated the diffusion layer, and traveled upwards to the upper surface of the flow channel (the transparent enclosure) due to buoyancy. Under this situation, more gas bubbles accumulated near the upper surface of the flow channel but did not hinder the access of methanol solution to the catalyst layer. However, for the horizontal cell orientation with the anode below the MEA ($\theta = 0°$), generated bubbles will accumulate near the upper surface of the flow channel (the diffusion layer), hindering the access of methanol solution to the catalyst layer and lowering the cell performance.

Figs. 9 and 10 show the effect of the cell orientations on the cell performance for the case when the methanol solution flow rate was increased to 1.0 and 8.0 ml min^{-1} while the other parameters were kept the same as the case shown in Fig. 7. The behavior similar to Fig. 7 can also be observed from Figs. 9 and 10: the best performance was achieved for the case of $\theta = 90°$, whereas the worst cell performance was obtained for the case of $\theta = 0°$. However, with increasing the methanol solution flow rate, the effect of the cell orientations on the cell performance became weaker, because the forced circulation furnished by the pump became larger than buoyancy at higher flow rates. This finding suggests that at low methanol flow rates, cautions have to be taken to the cell orientation to ensure high cell performance.

3.3. Effect of the methanol solution flow rate

The effect of the methanol solution flow rate on the cell performance at a low operating temperature of 23 °C is shown in Fig. 11. The experiments were conducted for the vertically-orientated cell ($\theta = 90°$) with 1 M methanol solution fed at flow rates of 0.25, 0.5, 1.0, 2.0, 4.0, and

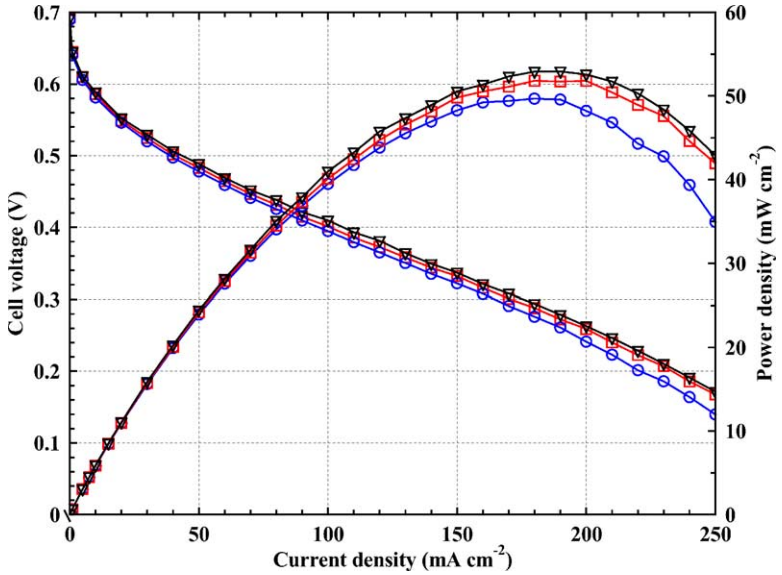

Fig. 9. Effect of cell orientation on the cell performance with 1 M methanol solution fed at 1.0 ml min^{-1} and at 60 °C (○, $\theta = 0°$; □, $\theta = 180°$; ▽, $\theta = 90°$).

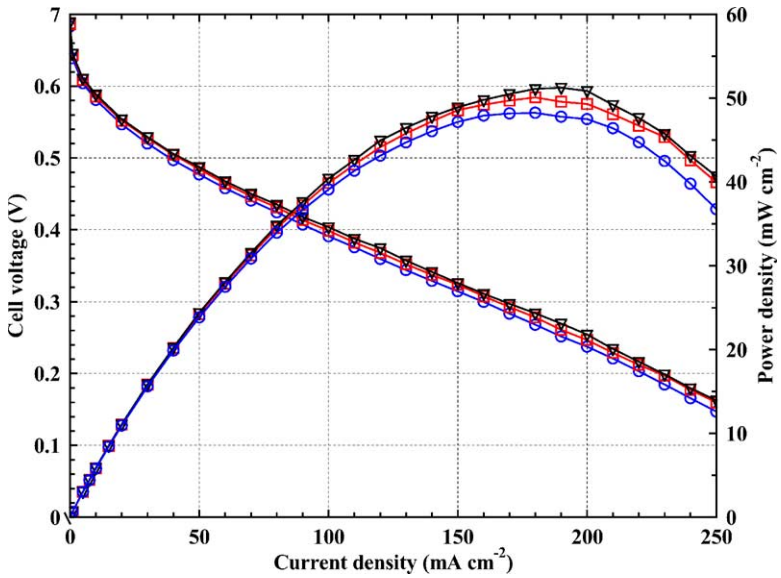

Fig. 10. Effect of cell orientation on the cell performance with 1 M methanol solution fed at 8.0 ml min^{-1} and at 60 °C (○, $\theta = 0°$; □, $\theta = 180°$; ▽, $\theta = 90°$).

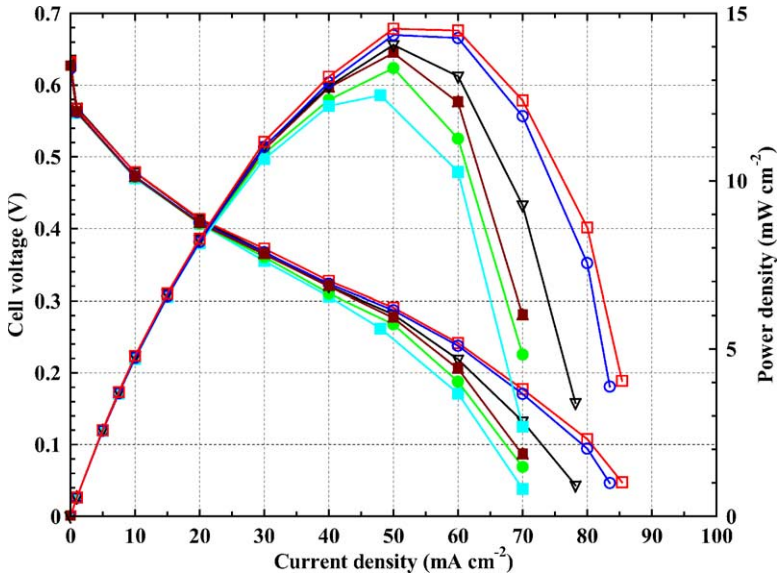

Fig. 11. Effect of the methanol solution flow rate on the cell performance for the vertical orientation ($\theta = 90°$) and using 1 M methanol solution at 23 °C (■, 0.25 ml min^{-1}, ○, 0.5 ml min^{-1}, □, 1.0 ml min^{-1}, ▽, 2.0 ml min^{-1}, ●, 4.0 ml min^{-1}, ■, 8.0 ml min^{-1}).

8.0 ml min^{-1}. As seen from Fig. 11, an increase in the methanol solution flow rate from 0.25 to 1.0 ml min^{-1} led to the improved cell performance. However, the cell performance became worse as the flow rate was further increased from 1.0 to 8.0 ml min^{-1}. This can be explained by the representative images of the gas CO_2 bubble behavior for the current density of 60 mA cm^{-2} as shown in Fig. 12(a–f), corresponding, respectively, to the methanol flow rates of 0.25, 0.5, 1.0, 2.0, 4.0, and 8.0 ml min^{-1}. A progressive scan of the six images in the Fig. 12 indicates that both the average bubble size and the quantity of CO_2 gas bubbles in the flow field were gradually reduced with increasing the methanol solution flow rate from 0.25 to 8.0 ml min^{-1}. For lower methanol solution flow rates of 0.25 and 0.5 ml min^{-1} shown in Fig. 12a and b, some long gas slugs were present in the flow field, which reduced the effective contact area between methanol and the gas diffusion layer and, thus led to poor cell performance. As the methanol solution flow rate was increased to 1.0 ml min^{-1}, as shown in Fig. 12c, the number of gas CO_2 bubble was reduced and the long gas slugs disappeared from the flow field because of the fact that the sweeping rate of the gas bubbles was increased with the methanol solution flow rate. As a result, an increased effective contact area between liquid methanol and the gas diffusion layer enhanced the mass transfer of methanol and hence, improved the cell performance as seen in Fig. 11.

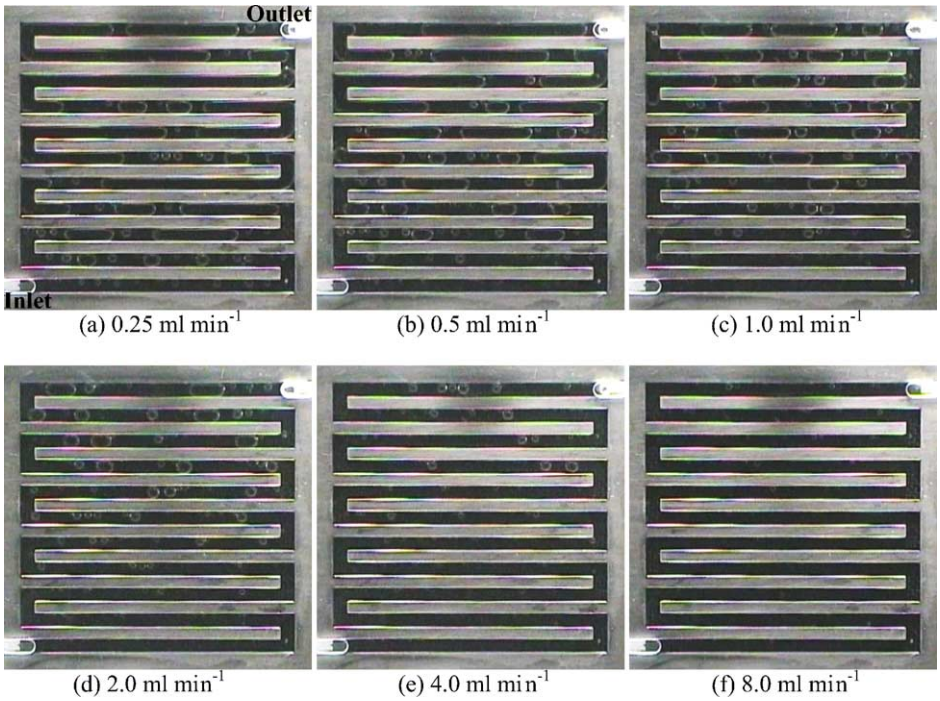

Fig. 12. CO_2 bubble behavior for different flow rates at 60 mA cm^{-2}, $\theta = 90^\circ$ and using 1 M methanol solution at 23 °C.

For the higher methanol solution flow rates of 2.0, 4.0, and 8.0 ml min^{-1}, as shown in Fig. 12(d–f), the quantity of gas CO_2 bubble decreased with increasing methanol solution flow rates. Under such a situation, the mass transfer of methanol was not a serious problem any more. However, an increase in the methanol solution flow rate is accompanied by an increase in the static pressure in the flow field. A higher static pressure tends to increase in the methanol crossover from the anode to the cathode, leading to deterioration in the cell performance. As seen from Fig. 11, the cell performance became worse and worse when the methanol solution flow rate was increased from 1.0 to 8.0 ml min^{-1}.

Figs. 13 and 14 show the effect of the methanol solution flow rates of 0.5, 1.0, 2.0, 4.0, and 8.0 ml min^{-1} on the cell performance when temperature was increased to 40 and 60 °C, but the other parameters were kept the same as the case shown in Fig. 11. It is seen that at a moderate operating temperature of 40 °C, the best cell performance was achieved at a flow rate of 1.0 ml min^{-1}, but either a lower flow rate (0.5 ml min^{-1}) or a higher flow rate (2.0, 4.0, and

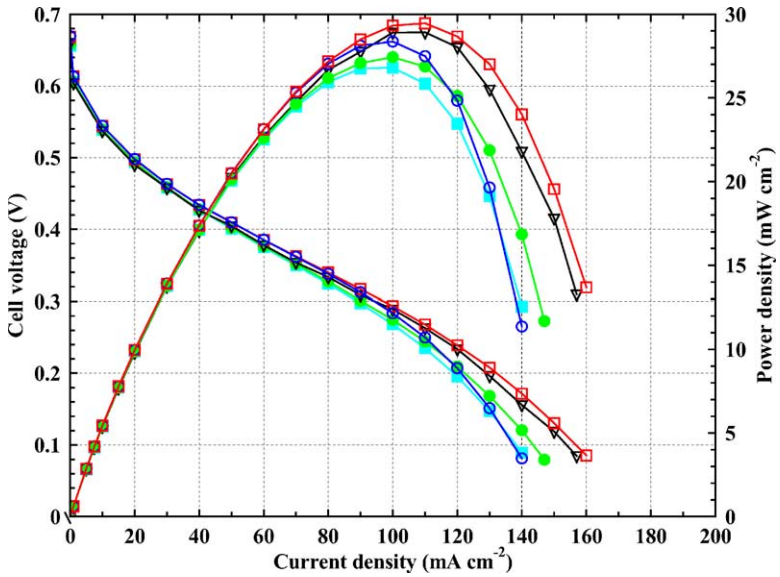

Fig. 13. Effect of the methanol solution flow rate on the cell performance for $\theta = 90^\circ$ and using 1 M methanol solution at 40 °C (○, 0.5 ml min^{-1}, □, 1.0 ml min^{-1}, ▽, 2.0 ml min^{-1}, ●, 4.0 ml min^{-1}, ■, 8.0 ml min^{-1}).

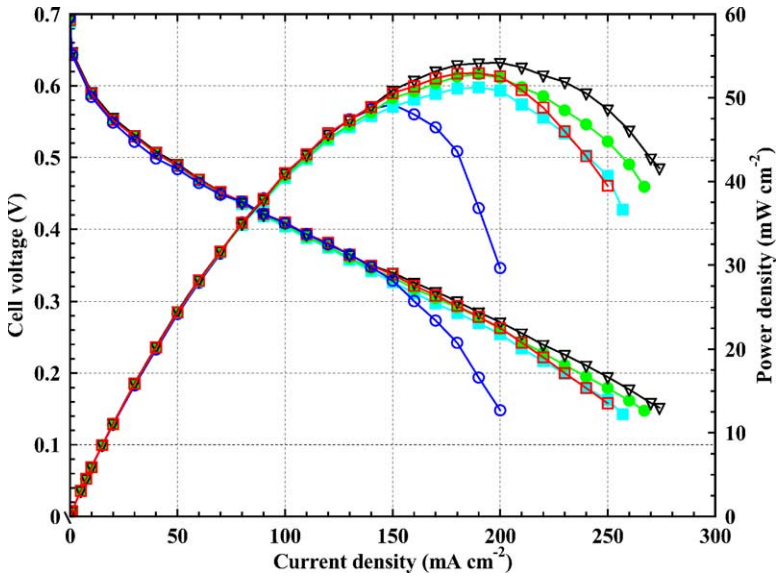

Fig. 14. Effect of the methanol solution flow rate on the cell performance for $\theta = 90^\circ$ and using 1 M methanol solution at 60 °C (○, 0.5 ml min^{-1}, □, 1.0 ml min^{-1}, ▽, 2.0 ml min^{-1}, ●, 4.0 ml min^{-1}, ■, 8.0 ml min^{-1}).

8.0 ml min^{-1}) led to a deterioration in the cell performance. Similarly, at a high operating temperature of 60 °C, an increase in flow rate from 0.5 to 2.0 ml min^{-1} improved the cell performance significantly, but a further increase from 2.0 to 8.0 ml min^{-1} resulted in a deterioration in the cell performance. Furthermore, a progressive scan of the cell performance curves shown in Figs. 11, 13 and 14, corresponding, respectively, to temperature of 23, 40, and 60 °C, indicates that the effect of the methanol solution flow rate on the cell performance became less sensitive with increasing the cell operating temperature. These experimental results revealed that the methanol solution flow rate has a significant effect on the cell performance, especially at low operating temperatures. This finding is significant for portable DMFCs that operate at room temperature. Cautions have to be taken to ensure an optimal flow rate to be designed for those DMFCs operating at low temperatures.

3.4. Effect of cell operating temperature

Fig. 15 shows the effect of temperatures on the cell performance for $\theta = 90^\circ$ and with 1 M methanol solution fed at 2.0 ml min^{-1}. As seen from this figure, the cell performance, including OCV, potential and power density increased with increasing temperature from 23 to 60 °C. The maximum power density was about 55 mW cm^{-2} at 60 °C. Fig. 16 shows the images of gas CO_2 bubble behavior at a selected current density of 80 mA cm^{-2} corresponding to the case

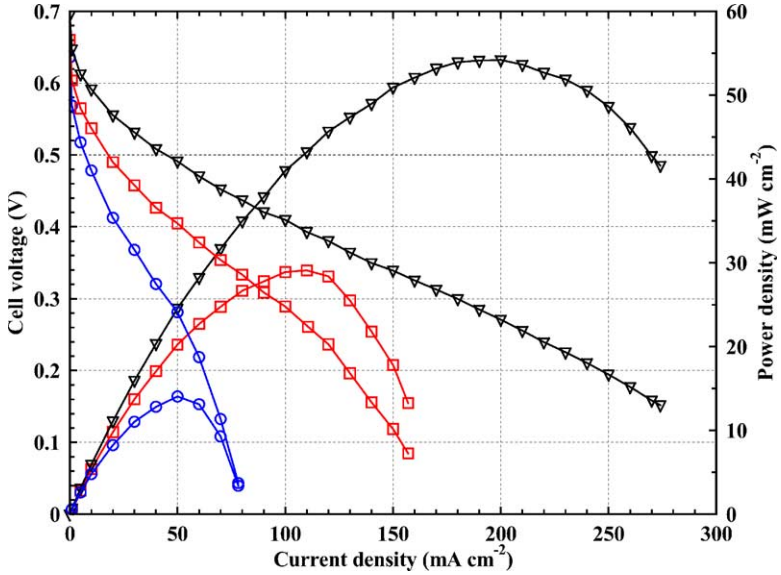

Fig. 15. Effect of temperature on the cell performance for $\theta = 90^\circ$ and with 1 M methanol solution fed at 2.0 ml min^{-1} (○, 23 °C, □, 40 °C, ▽, 60 °C).

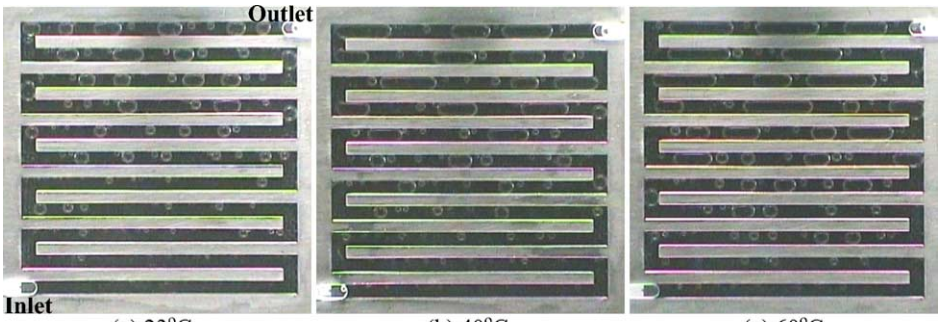

Fig. 16. Effect of temperature on the CO_2 bubble behavior for $\theta = 90^\circ$ at 80 mA cm^{-2} with 1 M methanol solution fed at 2.0 ml min^{-1}.

in the Fig. 15. As can be seen from the images shown in Fig. 16(a–c), the quantity of CO_2 gas bubbles in the flow field increased gradually with increasing the cell operating temperature from 23 to 60 °C. As indicated by Eq. (4), the quantity of gas CO_2 depends on the current density for a given temperature. However, the images shown in Fig. 16 indicate that the quantity also depends on the cell temperature at a fixed current density. There are two reasons associated with this phenomenon. First for a given static pressure (depending on the methanol solution flow rate), the CO_2 solubility in the aqueous methanol solution decreases with increasing temperature, thereby resulting in more CO_2 gas bubbles in the flow field at a higher temperature. Secondly, based on the ideal gas equation of state, the specific volume of CO_2 increases with temperature, also leading to the presence of a larger volume of gas CO_2 in the flow field. As a matter of fact, with the aid of the ideal gas equation of state:

$$\rho_{CO_2} = pM_{CO_2}/RT \tag{5}$$

Eq. (4) can be recast as:

$$q_{CO_2} = \frac{AR}{6Fp} iT \tag{6}$$

Based on Eq. (6), it can be estimated that for the MEA area of 4.0×4.0 cm^2 in this work at a given current density, the increase in temperature from 23 to 60 °C would cause an increase in the volume of gas CO_2 by about 12.5%.

It is also interesting to note from Fig. 16 that for a fixed current density, the average size of the bubbles in the flow field increased with temperature. This phenomenon is related to surface tension of methanol solution, which decreases with temperature. Thus, small bubbles tended to coalesce with each other and to form larger bubbles. In addition, the evaporation of methanol solution at a higher temperature might also contribute to this phenomenon. As can be seen in Fig. 16(a-c) at the current density of 80 mA cm^{-2}, gas slugs gradually became predominated in the flow field with increasing temperature. When the temperature reached to 60 °C, plenty of gas slugs formed and led to a reduced effective contact area between liquid methanol solution and the gas diffusion layer, causing a negative effect on the cell performance. However, an increase in temperature not only increases the activity of the catalysts, but also leads to a higher diffusion coefficient of methanol, both of which are favorable for improving the cell performance. This indicates that the increase in both the catalyst activity and mass transfer coefficient of methanol caused by the increase in temperature suppress the negative effect of large gas slugs formed at high temperatures.

4. Conclusions

A visual investigation of CO_2 gas bubble behavior inside the anode flow field consisting of a single serpentine channel has been performed. The experiments have shown that in the anode flow field there exist various two-phase flow patterns of gas CO_2 and methanol solution that vary with the cell operating conditions. The quantity of gas CO_2 bubbles in the flow field increased with the current density. At low current densities, small discrete bubbles appeared in the flow field. At moderate current densities, a number of gas slugs formed in addition to small discrete bubbles. And at high current densities, the flow field was predominated by rather long gas slugs. It has been shown that the presence of long gas slugs in the flow field led to a determination in the cell performance. The experiments also indicate that the cell orientation has a significant effect on the cell performance, especially at low methanol flow rates; for the present flow field design the best cell performance can be obtained when the cell is orientated vertically. This visually study shows that an increase in the methanol solution flow rate might tend to reduce the average size and the number of gas slugs in the flow field, thereby enhancing the methanol mass transfer. However, high flow rates may lead to an increased methanol crossover, resulting in deterioration in the cell performance. It has also been revealed that the effect of the methanol solution flow rate became more pronounced at low temperatures. Therefore, for portable DMFCs that operate at room temperature, special caution has to be taken for determining an optimal flow rate. The study on the effect of temperatures reveals that the cell performance got improved with increasing temperature, although large gas slugs formed in the flow field at high temperature. Furthermore, for the present flow field consisting of a single serpentine channel, channel-blocking phenomenon caused by

CO_2 gas slugs were never found for all the test conditions in this work.

Acknowledgements

The work described in this paper was fully supported by a grant from the Research Grants Council of the Hong Kong Special Administrative Region, China (Project No. HKUST6178/00E).

References

[1] C.K. Dyer, J. Power Sources 106 (2002) 31–34.
[2] T. Schultz, Su Zhou, Kai Sundmacher, Chem. Eng. 24 (2001) 12.
[3] R. Dillon, S. Srinivasan, A.S. Aricò, V. Antonucci, J. Power Sources 127 (2004) 112–126.
[4] J.P. Meyers, J. Newman, J. Electrochem. Soc. 149 (6) (2002) A710–A717.
[5] J.P. Meyers, J. Newman, J. Electrochem. Soc. 149 (6) (2002) A718–A728.
[6] J.P. Meyers, J. Newman, J. Electrochem. Soc. 149 (6) (2002) A729–A735.
[7] K. Scott, W.K. Taama, P. Argyropoulos, J. Power Sources 79 (1999) 43–59.
[8] H. Dohle, J. Divisek, R. Jung, J. Power Sources 86 (2000) 469–477.
[9] A.H. Wang, C.Y. Wang, J. Electrochem. Soc. 150 (4) (2003) A508–A519.
[10] G.Q. Lu, C.Y. Wang, T.J. Yern, X. Zhang, Electrochim. Acta 49 (2004) 821–828.
[11] J. Yu, P. Cheng, Z. Ma, B. Yi, J. Power Sources 124 (2003) 40–46.
[12] J.C. Amphlett, B.A. Peppley, E. Halliop, A. Sadiq, J. Power Sources 96 (2001) 204–213.
[13] Z. Qi, A. Kaufman, J. Power Sources 110 (2002) 177–185.
[14] Z. Qi, M. Hollett, C. He, A. Attia, A. Kaufman, Electrochem. Solid-State Lett. 6 (2) (2003) A27–A29.
[15] J. Nordlund, A. Roessler, G. Lindbergh, J. Appl. Electrochem. 32 (2002) 259–265.
[16] A. Blum, T. Duvdevani, M. Philosoph, N. Rudoy, E. Prlrd, J. Power Sources 117 (2003) 22–25.
[17] H. Dohle, R. Jung, N. Kimiaie, J. Mergel, M. Müller, J. Power Sources 124 (2003) 371–384.
[18] R. Jiang, D. Chu, J. Electrochem. Soc. 151 (1) (2004) A69–A76.
[19] N. Nakagawa, Y. Xiu, J. Power Sources 118 (2003) 248–255.
[20] X. Ren, T.E. Springer, T.A. Zawodzinski, S. Gottesfeld, J. Electrochem. Soc. 147 (2) (2000) 466–474.
[21] M.M. Mench, S. Boslet, S. Thynell, J. Scott, C.Y., Wang in: Proceedings of the Symposium on Direct Methanol Fuel Cells, The 199th Electrochem. Soc. Proc. Series, Princeton, NJ, 2001.
[22] P. Argyropoulos, K. Scott, W.M. Taama, Electrochim. Acta 44 (1999) 3575–3584.
[23] K. Scott, P. Argyropoulos, P. Yiannopoulos, W.M. Taama, J. Appl. Electrochem. 31 (2001) 823–832.
[24] T. Bewer, T. Beckmann, H. Dohle, J. Mergel, D. Stolten, J. Power Sources 125 (2004) 1–9.
[25] J. Ihonen, F. Jaouen, G. Lindbergh, G. Sundholm, Electrochim. Acta 46 (2001) 2899–2911.
[26] D.P. Davies, P.L. Adcock, M. Turpin, S.J. Rowen, J. Power Sources 86 (2000) 237–242.
[27] D.P. Davies, P.L. Adcock, M. Turpin, S.J. Rowen, J. Appl. Electrochem. 30 (2000) 101–105.
[28] E. Middelman, W. Kout, B. Vogelaar, J. Power sources 118 (2003) 44–46.
[29] J.G. Collier, J.R. Thome, Convective Boiling and Condensation, third ed., Clarendon Press,Oxford, 1994, pp. 9–29.
[30] P. Scharlin, R.W. Cargill et al., Carbon Dioxide in Water and Aqueous Electrolyte Solutions, Oxford University Press, Oxford, UK, 1996, pp. 1–13, 84–134.
[31] D. Chisholm, Two-Phase Flow in Pipelines and Heat Exchangers, George Godwin, Londin/New York, pp. 8–23.